NANO LETTERS

2006
Vol. 6, No. 9
1852−1857

Instability and Transport of Metal Catalyst in the Growth of Tapered Silicon Nanowires

Linyou Cao,[†] Bora Garipcan,[†,‡] Jennifer S. Atchison,[†] Chaoying Ni,[§] Bahram Nabet,[†,||] and Jonathan E. Spanier*[,†,||]

Department of Materials Science and Engineering, Drexel University, Philadelphia, Pennsylvania 19104, Department of Chemical Engineering, Bioengineering Divison, Hacettepe University, Beytepe, Ankara, 06800 Turkey, Department of Materials Science and Engineering, University of Delaware, Newark, Delaware 19716, and Department of Electrical and Computer Engineering, Drexel University, Philadelphia, Pennsylvania 19104

Received March 8, 2006; Revised Manuscript Received June 28, 2006

ABSTRACT

During metal-catalyzed growth of tapered silicon nanowires, or silicon nanocones (SiNCs), Au–Si eutectic particles are seen to undergo significant and reproducible reductions in their diameters. The reductions are accompanied by the transfer of eutectic droplet mass to adjacent, initially metal catalyst-free substrates, producing secondary nucleation and growth of SiNCs. Remarkably, the catalyst particle diameters on the SiNCs grown on the adjacent substrates are strongly correlated with those on the SiNCs grown on the initially Au-nanoparticle-coated substrate. These post-growth nanoparticle sizes depend on temperature and are found to be independent of the initial nanoparticle sizes. Our modeling and analysis indicates that the size reduction and mass transfer could be explained by electrostatic charge-induced dissociation of the droplet. The reduction in size enables the controlled growth of SiNCs with tip sharpnesses approaching the atomic scale, indicating that metal-catalyst nanoparticles can play an even more dynamic role than previously thought, and suggesting additional modes of control of shape, and of nucleation and growth location.

Though the role of the vapor−liquid−solid (VLS) mechanism in the growth of silicon whiskers was identified more than 30 years ago,[1] VLS has emerged within the past decade as one of the important methods of preparing one-dimensional inorganic nanostructured materials.[2−4] Its application in realizing one-dimensional (1D) nanostructures is considered to be highly promising for scalable, economical, and controllable growth of a variety of elemental and compound 1D nanostructures. In metal-catalyzed vapor-phase nanowire growth, it is well known that selection of catalyst particle diameter, growth temperature and pressure, precursor chemistry and flow rates can be used to control nanowire diameter, to control crystallographic growth direction, and to control composition and/or doping in either axial and radial directions[5−9] for the fabrication of novel nanodevices.[10−12] Growth conditions can also be manipulated to produce a wide variety of related 1D nanostructures with unique chemical, electronic, and functional properties. Among these related 1D nanostructures are tapered nanowires, silicon and germanium nanocones (SiNCs and GeNCs). These SiNCs and GeNCs can be produced with controlled apex angles and in different polymorphs.[13] Recently, these SiNCs and GeNCs have been shown to possess remarkable optical scattering properties.[14] In general, conical nanostructures have potential application in field emitters,[15] antennas,[16] and in scanning probe or nanomanipulation tools.[17]

The most important component in the VLS process is the liquid phase through which an adsorbed precursor gas-phase species diffuses and precipitates as solid atoms at the liquid−solid (L−S) interface, producing nanowire growth. The physicochemical properties of the catalyst droplet, for example, its eutectic temperature, thermodynamic properties, and size are known to strongly influence surface structure, nanowire diameter, and growth rate of the nanostructures.[5,7,18−21] Though the detailed role of catalyst particles as eutectic droplets or solid particles in the growth of nanowires has been elucidated by several groups, including, for example, in situ transmission electron microscopy (TEM) studies of the growth of Ge nanowires[22] and of Si nanowires,[23] an identification of the vapor−solid−solid (VSS) and surface-diffusion mechanisms in the metal-catalyzed

* To whom correspondence should be addressed. E-mail: spanier@drexel.edu.
[†] Department of Materials Science and Engineering, Drexel University.
[‡] Hacettepe University.
[§] University of Delaware.
[||] Department of Electrical and Computer Engineering, Drexel University.

10.1021/nl060533r CCC: $33.50
Published on Web 08/03/2006

growth of binary semiconductor nanowires[24] and elemental nanowires,[23] the dynamic behavior of nanodroplets and its effect on the growth of nanowires and related structures remains an area of active investigation.[23−26] Understanding the possible dynamics of the catalyst droplet and its application can lead to novel ways of controlling, for example, nanostructure diameter and shape[23] or growth location. Additional control may be enabled when coupled with, for example, electric field-assisted oriented growth.[27]

In this letter, we report an unexpected and dynamic behavior of catalyst nanoparticles in which Au-catalyst nanoparticles are seen to undergo reproducible diameter reduction during growth of SiNCs via chemical vapor deposition (CVD). Significantly, the reductions are accompanied by evidence of transport of eutectic droplets, leading to secondary nucleation and growth of SiNCs. We consider several possible mechanisms for the observed droplet dynamics and present corresponding model calculations. Our analysis indicates that the size reduction and mass transfer may be understood in terms of an electrostatic charge-induced breakup of the catalyst droplet, in which the force due to Coulomb repulsion exceeds that due to the surface tension of the droplet. Significantly, the reduction in size enables the growth of SiNCs with tip sharpnesses approaching the atomic scale, indicating that metal-catalyst nanoparticles can play an even more dynamic role than thought previously and shown recently,[23] suggesting additional possible modes of control of nanostructure shape, size, and growth location.

The detail of the synthesis of SiNCs via gold-catalyzed CVD has been described elsewhere.[13] Briefly, in a typical preparation evaporated 2-nm-thick Au films or Au colloids (Ted Pella, with diameters as indicated in the text) cast on poly-L-lysine-functionalized 300-nm SiO_2-coated Si(100) substrates were exposed to flowing precursor of 10% SiH_4 in He, ∼100 sccm, and carrier gas of N_2 or 5% H_2 in Ar, ∼100 sccm at selected temperatures from 500 to 700 °C under ∼5 Torr in a quartz tube furnace for 5−150 min. In addition, identical 300-nm SiO_2-coated Si(100) substrates without organic and Au catalyst ("blank control substrates") were placed in the growth furnace both upstream and downstream of each functionalized and Au-coated substrate with a spacing less than 0.5 mm between their edges and those of the functionalized and Au-coated substrates. SiNCs were characterized by scanning electron microscopy (SEM: FEI-XL30 and Amray 1850 field emission), energy-dispersive X-ray spectroscopy (EDS), and transmission electron microscopy (TEM, JEOL 2010F). TEM samples were prepared by sonicating the SiNCs from growth substrates in ethanol and dropping onto Ni or Cu TEM grids. With respect to the 2-nm-thick evaporated Au films, SEM and TEM analysis confirms that our annealing pretreatment results in the formation of 50−60-nm-diameter Au islands (not shown); these islands subsequently serve as catalytic sites for nanostructure nucleation and growth.

An SEM image of a typical SiNC grown using 20-nm-diameter Au catalyst nanoparticles is shown in Figure 1a, along with representative high-resolution TEM (HRTEM)

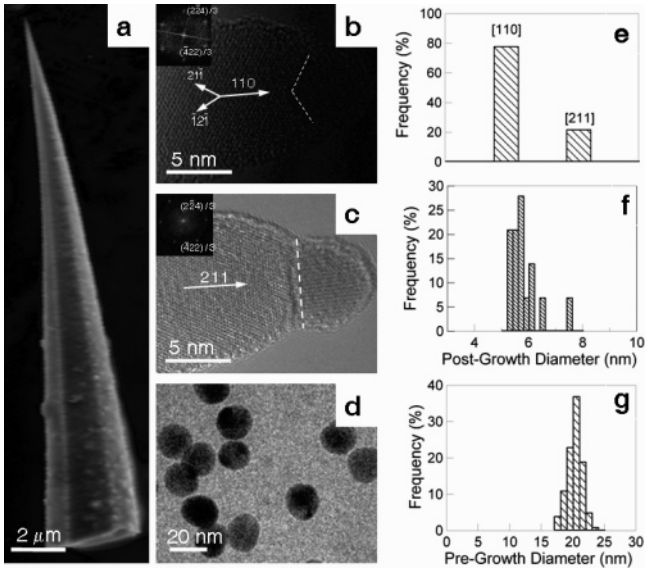

Figure 1. (a) SEM image of a SiNC synthesized with gold colloids as catalysts. HRTEM image of tips of the SiNCs as well as indexed corresponding Fourier transformation patterns with the direction for the axial growth being (b) ⟨110⟩ and (c) ⟨211⟩, as denoted using white arrows in these figures. (d) TEM image of the catalyst of original gold colloids. Histograms of (e) the predominant axial growth direction of the SiNCs, of (f) the size distribution of the final particles remaining at the SiNC tips, and of (g) the original gold colloidal particles for the same experimental conditions.

images of two characteristic crystallographic types of tips of the SiNCs and their corresponding 2D Fourier transformations in Figure 1b and c. Figure 1d is a representative TEM image of the Au nanoparticles from the same batch as those used in the growths. The lattice peaks shown in Fourier transformation pattern of the SiNCs (insets, Figure 1b and c) indicate that the main axis of each SiNC is predominantly either ⟨110⟩ or ⟨211⟩. Detailed characterizations and analyses of 40 SiNCs reveal that the main axis of the SiNC is along ⟨110⟩ in ∼80% of the SiNCs, with the remainder possessing a main axis along ⟨211⟩ (Figure 1e), consistent with the result for Si nanowires of diameter in the range of 3−10 nm.[28] These HRTEM images show that the interface between alloy/solid SiNC is (211) and that the ⟨110⟩ growth direction results from a combination of two (211) planes at the catalyst/SiNW interface forming a convex V-shaped morphology. The dominance of (211) at the interface instead of the lowest-free-energy (111) as reported in silicon whiskers[1] and nanowires[28] suggests that the adsorption and precipitation of Si atoms at higher temperature (∼650 °C) occurs under kinetic control because the growth rate of (211) is higher than that for (111) or (110) because of its lower atomic density.

Inspection of typical Au catalyst particles prior to (Figure 1d) and following (Figure 1b and c) SiNC growth at 650 °C reveals significant changes in diameter, with the original Au colloid diameters ranging from ∼17−24 nm, and the particles measured on the SiNC tips following growths are in the range of ∼5−8 nm. Analysis based on TEM and HRTEM images collected from more than 100 particles prior to, and 30 following, growth of SiNCs indicates the average diameter of the particles prior to growth; 20.2 ± 1.2 nm (Figure 1f)

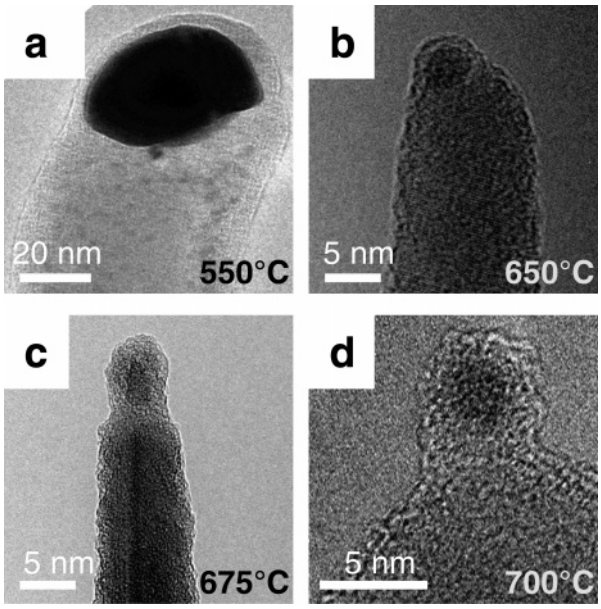

Figure 2. TEM images of representative catalyst particles following the 60-min CVD procedure using temperatures of (a) 550 °C, (b) 650 °C, (c) 675 °C, and (d) 700 °C, showing correlation of growth temperature with representative post-growth catalyst particle diameter.

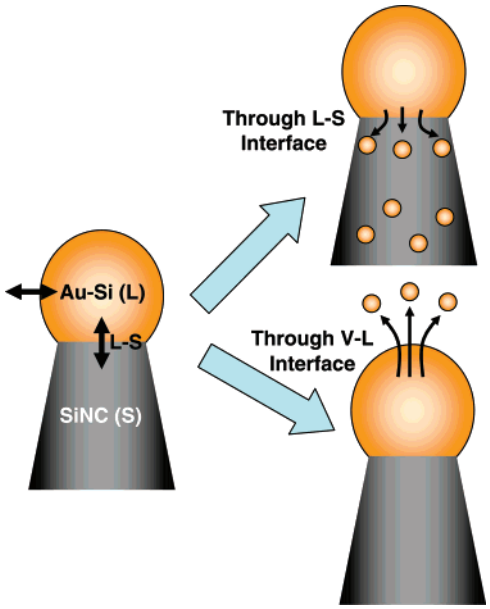

Figure 3. Schematic illustration of possible pathways for Au mass loss in the VLS process of SiNCs growth, which involves three phases (solid SiNC, liquid Au−Si, as well as the vapor phase flow) and two interfaces [liquid−solid (L−S) and vapor−liquid (V−L)]. Possible pathways for mass loss through the L−S interface are entrapment of bulk gold cluster, solution of gold atoms into solid SiNCs, and surface diffusion of Au atoms; those through the V−L interface the pathways include evaporation and droplet breakup.

is reduced to 5.82 ± 0.59 nm (Figure 1g) following a typical growth. Au colloids were also exposed to identical growth conditions, but with different carrier gases (H_2 and N_2), producing essentially similar results with respect to diameter reduction. Finally, the Au particles were exposed to the identical temperature, base vacuum pressure, and carrier gas flow rates, but without SiH_4, producing no observable changes in the diameters.

The nanoparticle diameters as observed following growth runs are seen to depend sensitively on temperature. Shown in Figure 2 is a series of TEM images of ∼50-nm-diameter Au catalyst nanoparticles collected from separate SiNCs following growths under identical conditions, but at different selected temperatures as shown. At process temperatures below 550 °C, no decrease in the sizes of the Au nanoparticles could be discerned (Figure 2a); these results were confirmed by several experiments under identically controlled conditions. At a growth temperature of 650 °C, the average post-growth diameter of the particles is observed to be ∼5 nm (Figure 2b), and smaller still (∼3 nm) for a higher growth temperature of 700 °C (Figure 2d). Though the particle sizes at 675 °C are comparable to those at 650 °C, the catalyst appears to be elongated along the axial direction of the SiNCs (Figure 2c). It is not clear whether this elongation is an intermediate state of the particle during the course of the shrinking or if it represents some quasi-equilibrium shape at the experimental temperature and pressure.

Additionally, a series of four growth runs were also performed using identical conditions at a growth temperature of 650 °C, except that Au nanoparticle size sets having initial diameters of 50, 20, 10, and 5 nm were selected. Significantly, the resulting catalyst particles at the tips of SiNCs for each value of initial diameter as determined by TEM were found to be approximately 5 nm in diameter in each case (not shown), suggesting the possibility of a critical size for these experimental conditions.

There are two possible paths for the reduction of catalyst mass: through the L−S and vapor−liquid (V−L) interfaces, as illustrated in Figure 3. At the L−S interface, Au catalyst atoms may be entrapped as one or more bulk clusters, or the atoms may become incorporated as a solid solution within the SiNC.[26] The entrapment of bulk gold clusters results from irregular growth of SiNCs and may be related, for example, to the presence of some impurities.[1] Recently, Hannon et al.[23] have shown using in situ TEM that the reduction in the sizes of catalyst particles can be due to surface diffusion of Au atoms along nanowire sidewalls and the substrate during the growth of ⟨111⟩-oriented Si nanowires. However, it appears highly unlikely that such processes can explain the observed narrow dispersion of post-growth diameters for a given growth temperature (Figure 1f). In addition, the model for surface migration of Au predicts that for ∼20-nm diameter Au catalyst particles, Si nanowire growths are limited to lengths of less than 1 μm.[23] In stark contrast, our SiNCs grown from 20-nm-diameter Au catalysts possess lengths that exceed 30 μm (Figure 1a). Taken together, these findings suggest that surface migration of Au is not likely to be a significant pathway of reduction in catalyst mass during the growth of SiNCs.

With respect to the possibility of incorporation as solid solution, because the maximum solubility of gold in silicon is no more than 2×10^{15} atoms/cm^3 at 650 °C,[29] the maximum number of solved gold atoms within a typical SiNC having a 2-μm-diameter base and a length of 20 μm can be no more than $\sim 1.4 \times 10^4$ atoms. This is an order of

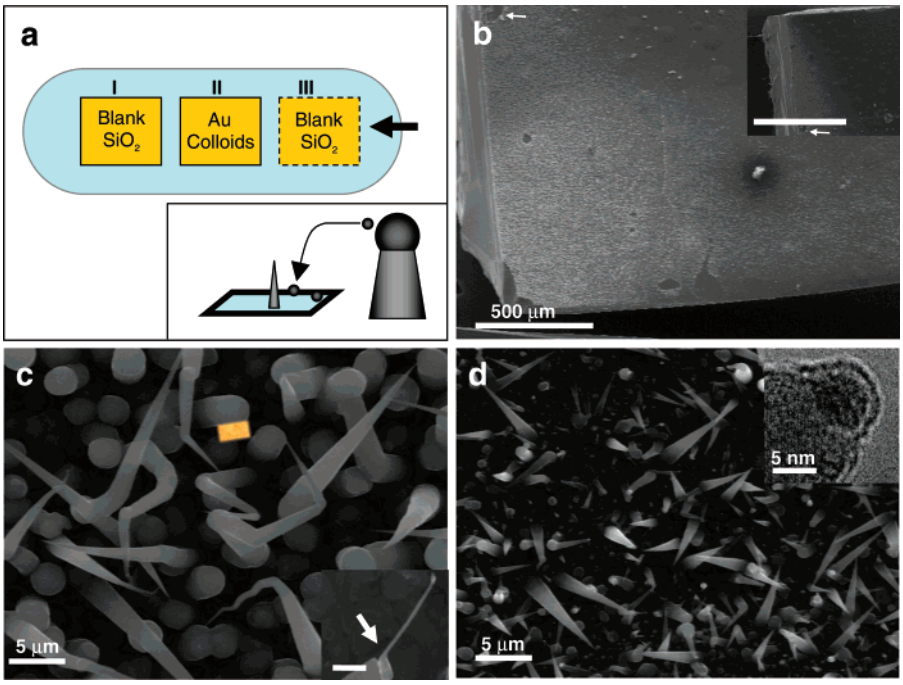

Figure 4. (a) Schematic depicting the relative placement of substrates in the furnace tube during the growth runs. The initially catalyst-free substrates were placed downstream (I) and upstream (III) in proximity to the location of the substrate containing Au catalyst nanoparticles (II). Inset: schematic illustrating the transfer of gold droplets. The arrow denotes the direction of gas flow. (b) Scanning electron microscopy (SEM) image of substrate I following a short growth run; the left edge corresponds to the edge closest to substrate II during the run; the inset is a lower-magnification SEM image of the area of this sample (scale bar corresponds to 1 mm). The general increase in number density of SiNCs approaching this edge can be discerned in the image. For reference, the white arrows in each image denote the same area on the sample. (c) SEM image of SiNCs grown on substrate II. Inset: a higher magnification SEM image of an individual SiNC from the same substrate; the white arrow denotes where change in diameter gas has taken place in the SiNC growth, and the scale bar corresponds to 200 nm. (d) SEM image of SiNCs grown on the initially Au catalyst-free substrate I. Inset, TEM image of an apex of a representative SiNC from substrate I.

magnitude smaller than the difference in the number of atoms between a 20-nm- and a 5-nm-diameter Au particle ($\sim 1.7 \times 10^5$). Our EDS analysis (JEOL 2010F) and mapping of a number of SiNCs from the tip to the base of each revealed no detectable Au signals using the Au L_α ($\sim$9.7 keV) and M_α ($\sim$2.3 keV) peaks as indicators except in the proximity ($\sim$100 nm) of the catalyst. Thus, even though the dissolution of Au atoms within the SiNCs through the L−S interface and/or the diffusion of Au atoms along the surface of the SiNCs may account for a portion of the loss of catalyst mass given the detection limit of EDS, one might also consider that a major contribution to the reduction in Au catalyst particle diameter may also occur through the V−L interface. In what follows, we describe experimental evidence of catalyst mass loss through the V−L interface, and model calculations pertaining to possible mechanisms. Specifically, we consider here mechanisms that involve either evaporation or droplet break-up (Figure 3). On the basis of our model calculations (see the Supporting Information) the decrease of the diameter caused by the evaporation of Au−Si alloy droplet in the present experiment is negligibly small. These calculations suggest that catalyst particles in our experiments instead lose mass primarily via breakup of the droplets.

As indicated above, our growth procedures involve the inclusion of blank control substrates placed adjacent to the functionalized and Au-coated substrates. Following the growth procedure, we find the reduction in catalyst diameters at the tips of the SiNCs on the functionalized substrates to be accompanied by the growth of smaller SiNCs on the initially blank substrates (Figure 4a−d). These findings suggest that the catalyst droplets break apart during growth, are transferred to the neighboring blank substrate, and subsequently catalyze the growth of SiNCs on the neighboring substrate. Furthermore, we observe in a number of samples that a sudden apparent change in the size of the SiNCs on the functionalized substrates occurs within the first few minutes of the growth of SiNCs when catalyzed by large ($\sim$50 nm) Au particles; an example is shown in the inset of Figure 4c. This breakup is believed to occur at the beginning of the growth because the resulting catalyst shows no obvious changes in size after more than 15 min of growth time. Significantly, HRTEM characterizations of the catalyst particles on the tips of the SiNCs on the initially blank substrates following growth at 650 °C reveal that they are also $\sim$5 nm in diameter (Figure 4d, inset).

The number density of SiNCs grown on the blank control substrates appears to depend on both the placement of the blank control substrates in relation to the Au nanoparticle-coated substrate as well as the specific location within the blank control substrates (Figure 4a). First, though SiNCs can be found on both blank control substrates at downstream (I, Figure 4a) and upstream (III, Figure 4a) locations with respect to the Au catalyst-containing substrate (II, Figure 4a), there is a higher number density of SiNCs on substrate I.

Second, the areas of highest number density of SiNCs grown on the blank control substrates are at and near the edges of these substrates closest to substrate II (Figure 4b). It may be that the cleaved edges possess a higher number of high-energy surfaces that favor adsorption of droplet particles and subsequent nucleation and growth of additional SiNCs. Similar transfer of the Au catalyst to the adjacent initially catalyst-free substrates and growth of SiNCs also occurred under different selected flow rates of SiH_4 ranging from ~50 to ~200 sccm. We note that at a SiH_4 flow rate of ~50 sccm, very low yields of nontapered nanowires were produced on both substrates II and I (not shown).

Accidental and random breakup of catalyst droplets caused by a lateral temperature gradient and/or a sudden change of temperature was reported by Wagner.[1] Furthermore, oversupply of Si vapor as well as interplay of surface energies of the wire and liquid droplet were also reported to cause the droplet to be unstable, leading to multiple nucleation[1] or oscillation in resulting structures.[23,25] However, to the authors' knowledge, experimental conditions under which the diameter of all catalyst droplets examined are reduced to temperature-dependent diameters with narrow dispersion suggestive of a temperature-dependent critical size has not been reported previously.

One may consider that gas flow in these experiments may be the cause of the droplet breakup, analogous to high-velocity gas flow-induced breakup of water droplets.[30] In this mechanism, the droplet deformation and breakup in the gas flow is governed by competition between hydrodynamic stresses (viscous and/or inertial), which act to deform the droplet, and surface tension, which opposes increase of the surface area, providing a driving force toward restoring ellipsoidally deformed objects to a spherical shape. However, our model calculations (see the Supporting Information) indicate that the gas flow itself cannot be the origin of breakup of a nanoscaled liquid metal alloy droplet. In what follows, we present a simple model of electrostatic charge-induced breakup that may account for our experimental results.

An electrically charged droplet can become unstable when repulsive electrostatic forces on its surface exceed surface tension forces, causing the droplet to break apart.[31,32] Assuming that charge is distributed uniformly at the surface of the droplet, the balance condition (the Rayleigh limit)[31] can be written $\epsilon_0 E_r^2/2 = 2\gamma/r_c$, where ϵ_0 is the dielectric constant of the environment, γ is the surface tension, r_c is the critical droplet radius, and E_r is the electric field at the droplet surface, which can be written in terms of the charge Q, $E_r = Q/4\pi\epsilon_0 r_c^2$. Thus, Q at the Rayleigh limit is given by $Q = 8\pi\sqrt{\epsilon_0 \gamma r_c^3}$. By substituting an appropriate value for γ (~0.85 N/m)[21] and taking $r_c = 3 \times 10^{-9}$m, Q is estimated to be 1.08×10^{-17} C, or ~68 electrons, corresponding to a value for E_r at the droplet surface of ~1.15 V/Å. This calculated value of E_r is comparable to that involved for the release of ions via liquid metal ion sources using liquid Au−Si alloys.[33]

A plot of the calculated charge per droplet expressed as the number of electrons as well as that for the resulting electric field at the surface as functions of critical diameter $2r_c$ is shown in Figure 5. In this model, the catalyst droplet acquires electrostatic charge during the CVD reaction, and at the point the Coulomb repulsion exceeds the surface tension force, it dissociates into smaller droplets, releasing charge and reducing the electrostatic force on the surface of the remaining droplet attached to the original SiNC. Because of obvious loss of the catalyst mass, the breakup is believed to follow a charged residue model[34] in which the parent droplet breaks into smaller daughter droplets carrying amounts of charge that are proportional to their relative size.

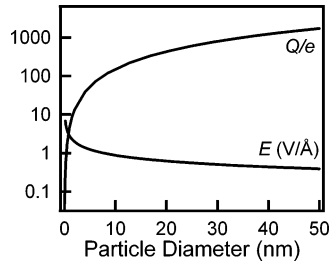

Figure 5. Calculated charge per droplet Q (expressed as a number of electrons), and electric field E (in V/Å) at the droplet surface at the Rayleigh limit as a function of the droplet diameter based on the model described in the text.

What evidence exists to support the hypothesis of this proposed charge accumulation as a precursor to droplet dissociation? If charge buildup occurs on alloy eutectic particles affixed to dopant-free and insulating SiNCs, then charge dissipation into the rest of the SiNC would be expected to be impeded by the barrier presented by the metal−insulator interface. Thus, the growth of *doped* SiNCs would provide a conductive pathway for charge to migrate from the droplet and into the SiNC tip and base, and supporting evidence of this hypothesis. In separate, but otherwise identical experimental conditions using metal catalysts and adjacent initially catalyst-free substrates, we introduced PH_3 as a dopant gas (1000 ppm in H_2) at 5 sccm along with 200 sccm of SiH_4 during the growth of SiNCs. For comparison, we also conducted growth runs with a catalyst-free substrate in the absence of any metal catalyst particle-coated substrate. As shown in Figure S1 of the Supporting Information, we find growth of SiNCs under in situ doping conditions on Au-catalyzed substrates (Figure S1a) to be completely suppressed on the adjacent, initially catalyst-free substrates (Figure S1b). The only structures that appear are due to growths of Si islands, which result from homogeneous decomposition of SiH_4 in the absence of any Au catalysts (Figure S1c).

How do Au−Si eutectic droplets become charged during metal nanoparticle-catalyzed and thermal decomposition-assisted CVD-growth of Si nanostructures? Investigations of fluid systems suggest several possible mechanisms for electrostatic charging in vapor−liquid−solid flow systems, including tribo-electrification, ion collection, thermionic emission, and frictional charging.[35] Specifically, it has been reported that Au nanoparticles placed in tube furnace flowing high-purity nitrogen become charged when they are heated to more than 600 °C,[36] and it has been proposed that the

decomposition of a similar process gas, SiH_2Cl_2, can produce charged silicon clusters in CVD;[37] in this latter work, the authors reported an abrupt increase in the ion current following the start of SiH_2Cl_2 decomposition. Our findings of temperature-dependent values of the reduced-diameters of the catalyst particles are consistent with temperature-dependent thermal-charging of gold nanoparticles and with the possibility of temperature-dependent partial decomposition of gaseous precursors into charged species and subsequent charge transfer from the vapor to liquid phases.

Further work is needed to validate the applicability of this model by providing additional experimental evidence of the charged droplet mechanism, and to quantify the possible temperature-dependent charge transfer from the gas phase to droplets under our experimental growth conditions. Nevertheless, we find conditions for reproducible decreases in temperature-dependent catalyst diameters during metal nanoparticle-catalyzed CVD of SiNCs, which are accompanied by the appearance of secondary nucleation and growth of SiNCs on adjacent blank control substrates. For a fixed growth temperature, final diameters are not seen to be correlated initial diameters; instead, we find evidence of the existence of temperature-dependent critical nanoparticle diameters common to both particles on the SiNCs and those on SiNCs grown on the blank control substrates following growths. Among the several possible mechanisms considered here, we demonstrate that only Coulomb repulsion and droplet dissociation can account for the observed results. Significantly, the reduction in size enables the growth of SiNCs with tip sharpnesses approaching the atomic scale, indicating that metal-catalyst nanoparticles can play a more dynamic role than previously thought, and suggesting additional modes of control of nanostructure shape and growth location.

Acknowledgment. We are grateful to Akos Vertes and Mark Reeves for technical discussions. J. S. gratefully acknowledges support at Drexel University from the U. S. Army Research Office under a Young Investigator Award (W911NF-04-100308) and from the Nano-Bio Interface Center (an NSF-NSEC) at the University of Pennsylvania and Drexel (DMR-0425780). B.G. acknowledges supported from TUBITAK-NATO A2 from Turkey and from the Department of Health of the Commonwealth of Pennsylvania.

Supporting Information Available: Model calculations. This material is available free of charge via the Internet at http://pubs.acs.org.

References

(1) Levitt, A. P. *Whisker Technology*; John Wiley & Sons: New York, 1970.
(2) Hu, J. T.; Odom, T. W.; Lieber, C. M. *Acc. Chem. Res.* **1999**, *32*, 435.
(3) Kong, J.; Cassell, A. M.; Dai, H. *Chem. Phys. Lett.* **1998**, *292*, 567.
(4) Law, M.; Goldberger, J.; Yang, P. *Annu. Rev. Mater. Res.* **2004**, *34*, 83.
(5) Gudiksen, M. S.; Lieber, C. M. *J. Am. Chem. Soc* **2000**, *122*, 8801.
(6) Lauhon, L. J.; Gudiksen, M. S.; Wang, D.; Lieber, C. M. *Nature* **2002**, *420*, 57.
(7) Cui, Y.; Lauhon, L. J.; Gudiksen, M. S.; Wang, J. F.; Lieber, C. M. *Appl. Phys. Lett.* **2001**, *78*, 2214.
(8) Cui, Y.; Duan, X.; Hu, J. T.; Lieber, C. M. *J. Phys. Chem. B* **2000**, *104*, 5213.
(9) Wang, Y. F.; Lew, K. K.; Ho, T. T.; Pan, L.; Novak, S. W.; Dickey, E. C.; Redwing, J. M.; Mayer, T. S. *Nano Lett.* **2005**, *5*, 2139.
(10) Huang, Y.; Duan, X.; Cui, Y.; Lauhon, L. J.; Kim, K.; Lieber, C. M. *Science* **2001**, *294*, 1313.
(11) Lu, W.; Xiang, J.; Timko, B. P.; Wu, Y.; Lieber, C. M. *Proc. Natl. Acad. Sci.* **2005**, *102*, 10047.
(12) Yang, C.; Zhong, Z. H.; Lieber, C. M. *Science* **2005**, *310*, 1304.
(13) Cao, L.; Laim, L.; Ni, C.; Nabet, B.; Spanier, J. E. *J. Am. Chem. Soc.* **2005**, *127*, 13782.
(14) Cao, L.; Nabet, B.; Spanier, J. E., submitted for publication, 2006.
(15) Bai, X. D.; Zhi, C. Y.; Liu, S.; Wang, E. G.; Wang, Z. L. *Solid State Commun.* **2003**, *125*, 185.
(16) Shavit, R. *IEEE Trans. Antennas Propag.* **1997**, *45*, 1086.
(17) Hashiguchi, G.; Goda, T.; Hosogi, M.; Hirano, K.; Kaji, N.; Baba, Y.; Kakushima, K.; Fujita, H. *Anal. Chem.* **2003**, *75*, 4347.
(18) Kikkawa, J.; Ohno, Y.; Takeda, S. *Appl. Phys. Lett.* **2005**, *86*, 123109.
(19) Tan, T. Y.; Li, N.; Gosele, U. *Appl. Phys. Lett.* **2003**, *83*, 1199.
(20) Sunkara, M. K.; Sharma, S.; Miranda, R.; Lian, G.; Dickey, E. C. *Appl. Phys. Lett.* **2001**, *79*, 1546.
(21) Schmidt, V.; Senz, S.; Gosele, U. *Appl. Phys. A* **2005**, *80*, 445.
(22) Wu, Y.; Yang, P. *J. Am. Chem. Soc* **2001**, *123*, 3165.
(23) Hannon, J. B.; Kodambaka, S.; Ross, F. M.; Tromp, R. M. *Nature* **2006**, *440*, 69−71.
(24) Persson, A. I.; Larsson, M. W.; Stenstrom, S.; Ohlsson, B. J.; Samuelson, L. *Nat. Mater.* **2004**, *3*, 677.
(25) Ross, F. M.; Tersoff, J.; Reuter, M. C. *Phys. Rev. Lett.* **2005**, *95*, 146104.
(26) Perea, D. E.; Allen, J. E.; May, S. J.; Wessels, B. W.; Seidman, D. N.; Lauhon, L. J. *Nano Lett.* **2005**, *6*, 181.
(27) Englander, O.; Christensen, D.; Kim, J.; Lin, L.; Morris, S. J. S. *Nano Lett.* **2005**, *5*, 705.
(28) Wu, Y.; Cui, Y.; Huynh, L.; Barrelet, C. J.; Bell, D. C.; Lieber, C. M. *Nano Lett.* **2004**, *4*, 433.
(29) Collins, C. B.; Carlson, R. O.; Gallagher, C. J. *Phys. Rev.* **1957**, *105*, 1168.
(30) Stone, H. A. *Annu. Rev. Fluid. Mech.* **1994**, *26*, 65−102.
(31) Rayleigh, L. *Philos. Mag.* **1882**, *14*, 184.
(32) Last, I.; Levy, Y.; Jortner, J. *Proc. Natl. Acad. Sci.* **2002**, *99*, 9107.
(33) Purcell, S. T.; Binh, V. T.; Thevenard, P. *Nanotechnology* **2001**, *12*, 168.
(34) Forbest, R. G. *Vacuum* **1996**, *48*, 85.
(35) Park, A.; Fan, L. S., unpublished work, 2006.
(36) Magnusson, M. H.; Deppert, K.; Malm, J.; Bovin, J.; Samuelson, L. *J. Nanopart. Res.* **1999**, *1*, 243.
(37) Hwang, N. M.; Jeon, I. D.; Kim, D. Y. *J. Ceram. Processing Res.* **2000**, *1*, 34.

NL060533R